A TUNEABLE WAVEGUIDE ARRAY FOR RADIATION & SCATTERING EXPERIMENTS

Ong Zhi Xuan[1], Wee Su-Rei[2], Tay Chai Yan[3], Chia Tse Tong[3]
[1]Temasek Junior College (Junior College), 22 Bedok South Road, Singapore 469278
[2]Dunman High School, 10 Tanjong Rhu Road, Singapore 436895
[3]DSO National Laboratories, 12 Science Park Dr, Singapore 118225

1.   Abstract

A 20x20 reconfigurable waveguide array with an interelement spacing of 0.67λ operating at 9.5GHz is presented. Each waveguide unit cell has an available phase range of 412°. The phase is varied by changing the depth of the metal reflector in the waveguide. The metal reflector is attached to an additively manufactured support. To reduce the number of dissimilar supports, the depth is quantised into a 3-bit system over a 360° phase range. Two configurations of the waveguide array are presented. First, for scattering control under plane wave illumination, a 10° incident wave is reflected to 45°. Second, for radiation control, the array is configured as a reflectarray to increase the boresight gain from an X band horn antenna. Measurements are conducted to verify the two cases.

2.   Introduction

Waveguides are components that restricts the propagation of electromagnetic waves to a specific direction. [1] They are commonly employed in high-performance radio frequency systems due to several benefits such as high gain, high efficiency, wide operational bandwidth, and high-power handling capacity. [2,3] Waveguide arrays employed as planar antennas thus feature negligible transmission loss in the millimetre waveband, and its simple, compact structure can reduce manufacturing complexity, unlike parabolic reflectors. [4,5]

An application of waveguide array is the reflectarray, which is an antenna that consists of an array of reflecting elements that introduce spatial phase shifts or time-delays to enable beam steering and beamforming capabilities [6] via the principle of superposition [7]. Conventionally, the effect of beam steering and beamforming is achieved with the use of phased arrays. However, phased arrays are notorious for their high complexity and cost, due to the use of expensive components like transceivers, microwave phase shifters, amplifiers and power dividers [8]. The use of power dividers can lead to power loss and antenna inefficiency [9]. Unlike phase arrays, reflectarrays do not require such components and thus, do not have such shortcomings [6].

In the development of reflectarrays, the reflecting elements employed can include dipoles, printed microstrip patches or rings, with a varied size or a varied phase delay lines [8]. Often, tuneable lumped elements, like pin diodes and varactors are used, to create a reconfigurable reflectarray antennas (RRAs) [10,11,12]. However, few studies exist in the implementation of tuneable metal waveguides into RRAs, which is investigated in this project. Although waveguides are previously criticised for having a bulky and heavy structure [8], this study introduces a novel method of utilising additive manufacturing, fused filament fabrication (FFF), to synthesise parts of the waveguide. Benefits of FFF includes cost savings from replacing fully metallic components with cheaper plastic filament and lighter overall weight, while producing models with dimensions of high precision [10].

3.   Aim

The aim of this project is to demonstrate the use of a reconfigurable waveguide array for scattering control and as a reflectarray antenna, while investigating its accuracy of beam-steering in a 3-bit quantisation scheme.

4.   Waveguide Array Design

4.1   Waveguide Unit Cell Design

The unit cell has dimensions of 20x20x30 mm^3 as shown in Figure 1. It comprises metal walls of 0.5 mm thickness, with open ends. Thus, a hollow region is 19x19x30 mm^3 where a plate support is inserted.
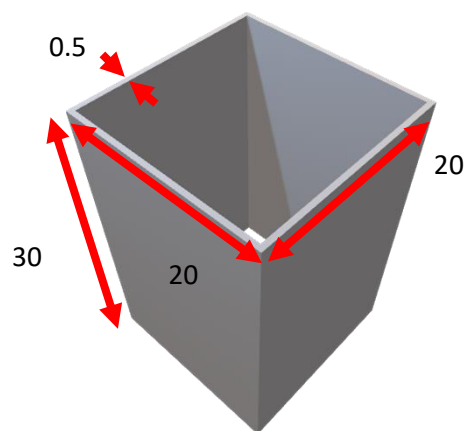
Figure 1: Unit cell wall (all dimensions in mm).

The plate support shown in Figure 2 is an inverted U-shaped structure that protrudes at the ends to hook onto the waveguide wall. It is made of Acrylonitrile Butadiene Styrene (ABS). A metal plate reflector of 19x19x1mm^3 is attached to the top surface.
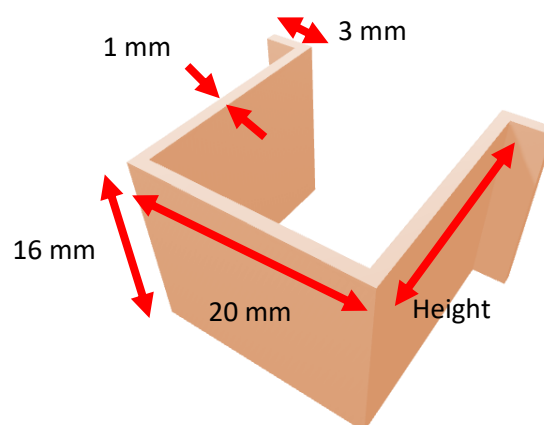

Figure 2: Plate support (arbitrary height)

To determine the operating frequency of the design, the cut-off frequency for each mode of propagation in the given waveguide cell is calculated via equation (1)

$$f_c = \frac{c}{2}\sqrt{\left(\frac{m}{a}\right)^2 + \left(\frac{n}{b}\right)^2}$$ (1)

where f_c is the cut-off frequency, c is the speed of light, a and b are the length and width of the waveguide cell respectively, and m and n are numbers representing the mode of propagation. The operating frequency of the waveguide cell is chosen at 9.5GHz, between the cut-off frequency of the TE_{10} and TE_{11} modes.

Table 1: Cut-off frequency of propagating modes for 20x20 mm^2 waveguide

Propagation Mode	Cut-off Frequency (GHz)
TE_{10} , TE_{01} (Dominant modes)	7.49
TE_{11} , TM_{11}	10.60
TE_{20}	14.99
TE_{12} , TE_{21} , TM_{21} , TM_{12}	16.76

Phase delay in the unit cell is achieved by varying the position of the metal reflector inside the waveguide. The unit cell is simulated in CST Microwave Studios to obtain the reflection phase as a function of the reflector depth, as shown in Figure 3. It has a maximum phase coverage of 412.66° at the centre frequency of 9.5GHz.
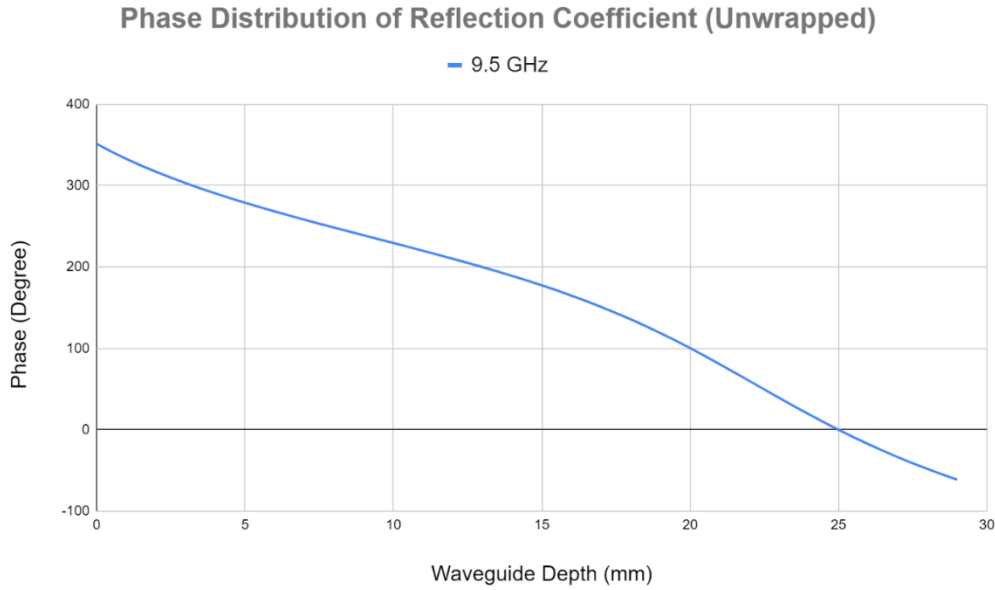

Figure 3: Phase vs depth.

4.2   Design of Waveguide Array for Scattering Control

The waveguide array consists of 20x20 unit cells for an overall dimension of 421x421x30 mm^3. For scattering control, the phase-shift required by each cell of the array is calculated via equation (2),

$$\varphi_r(x,y) = k[-(x_n \cos\varphi_i + y_n \sin\varphi_i)\sin\theta_i - (x_n \cos\varphi_s + y \sin\varphi_s)\sin\theta_s]$$ (2)

3

where $k = 2\pi/\lambda$ (wave propagation constant), x_n and y_n are the position coordinates of the nth unit cell, φ_i and θ_i are the spherical coordinates of the incident plane wave, φ_s and θ_s are the spherical coordinates of the scattered beam direction. From Figure 3, the phase-shift required for each cell is converted into the corresponding waveguide depth. For ease of tunability, a 3-bit quantisation was adopted for the phase (corresponding to 45° intervals), resulting in 8 different depths.

4.3   Design of Waveguide Array for Radiation

In this case, a feedhorn is positioned at 0.26 m above the waveguide array (for an F/D of 1.22) such that edge taper is at -10dB to reduce diffractions [13]. Equation (2) is modified as follows:

$$\varphi_r(x, y) = k[d_i - (x_n \cos \varphi_r + x_r \sin \varphi_r) \sin \theta_r] \tag{3}$$

where φ_r and θ_r are the spherical coordinates of the radiated beam direction.

5.   Fabrication of Waveguide Array Prototype

The measurement support for the prototype shown in Figure 4 consists of 3 wooden boards, assembled in an L-shape, with an extension at the front to support the feedhorn for radiation experiment. For the waveguide array, an egg crate metal grille is used. In each waveguide cell, an aluminium plate is glued onto an additively manufactured support as shown in Figure 5. Supports of 8 different heights shown in Figure 3 for the 3-bit quantisation scheme.
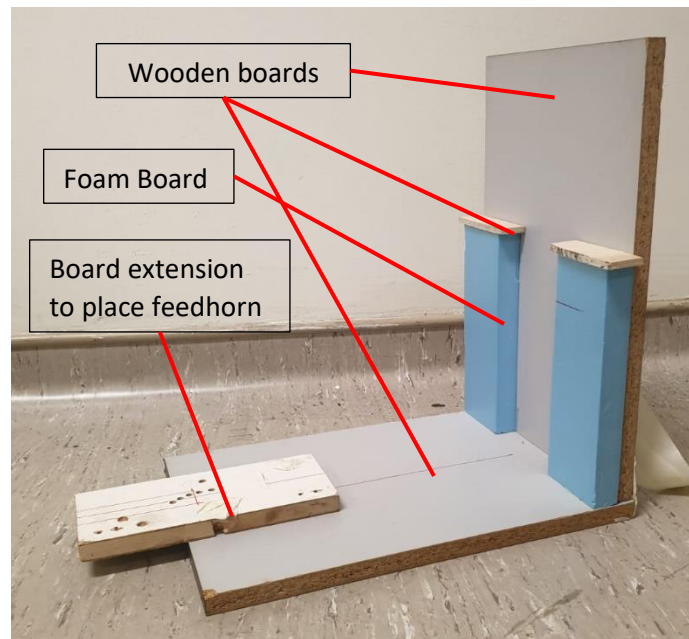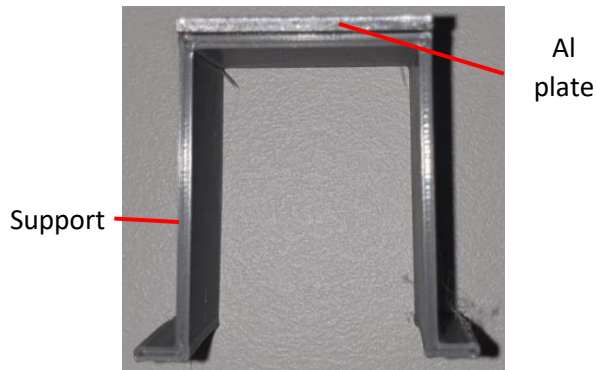

Figure 4: Waveguide array support.
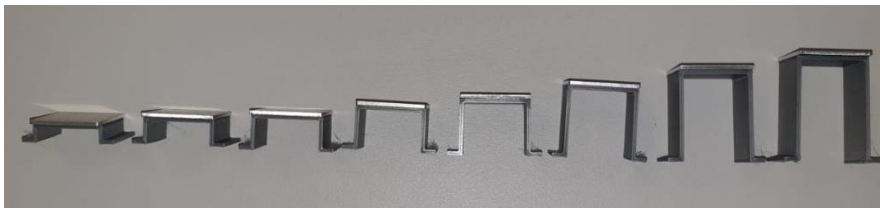
Figure 5: Metal plate on support.

Figure 6: 8 supports of varying heights.

The supports with Al plates are slotted into the waveguide array according to the required quantized phase. The array is tied to the measurement support as shown in Figure 7.
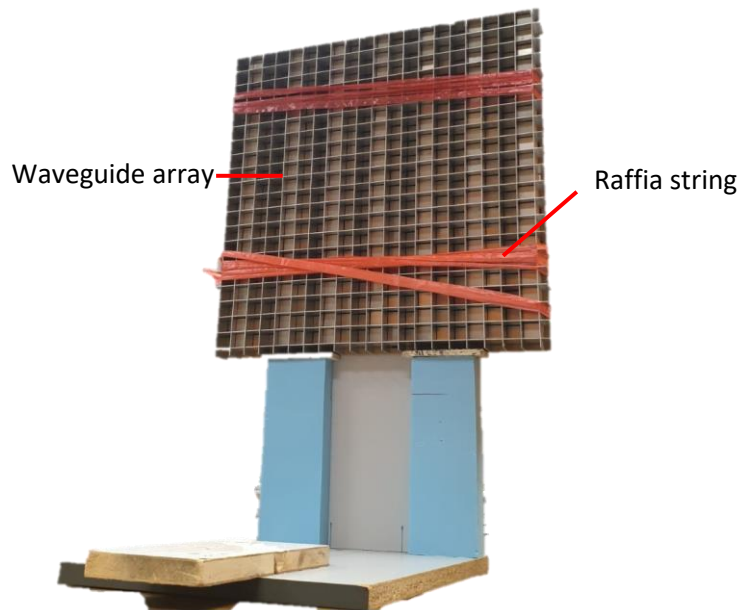

Figure 7: Physical prototype for scattering measurement.

For radiation measurements, a feedhorn shown in Figure 8 is attached to the front of the array prototype to provide illumination.
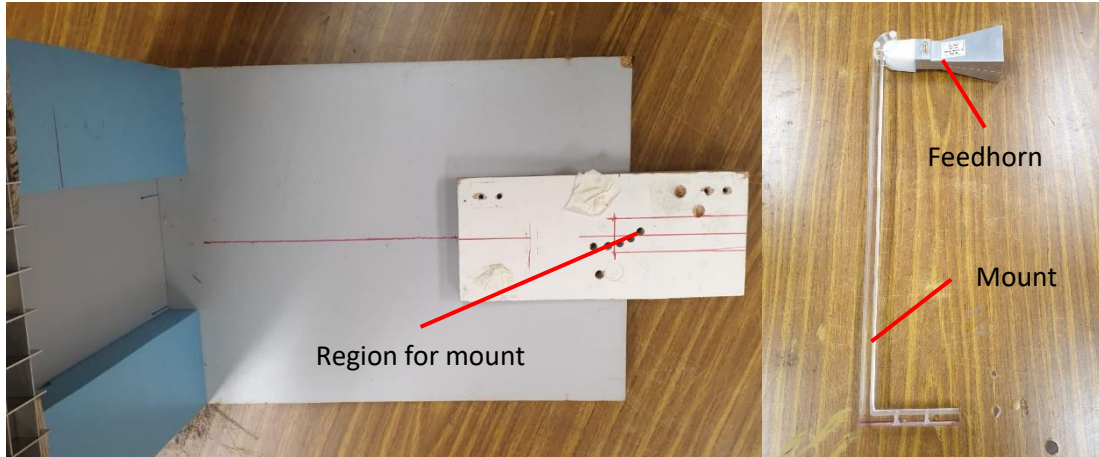
Figure 8: (Left) top view of array and measurement support; (Right) feedhorn & mount.

6. Results and Discussion

6.1 Scattering

6.1.1 Case 1: $\phi_i = 0°, \theta_i = 0°; \phi_s = 0° \theta_s = 10°$

A bistatic radar cross section (RCS) of the scattering array was simulated in CST as shown in Figure 9. The array was designed to deflect a normal incident plane wave to 10° off normal. The quantised (Q) and unquantized (U) models produce similar results.
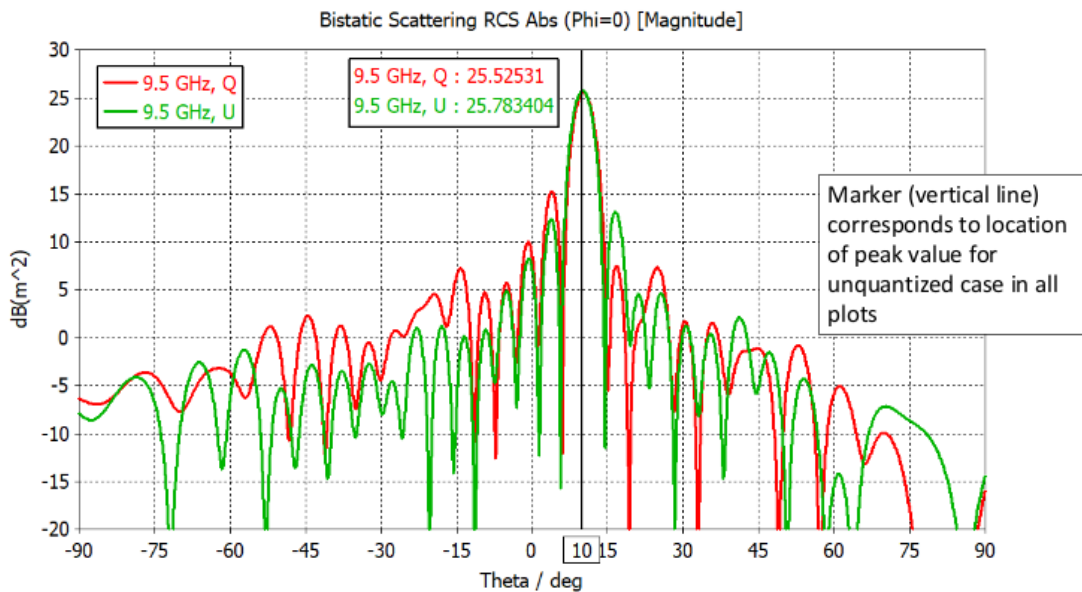

Figure 9: Simulated bistatic RCS of waveguide array ($\phi_i = 0°, \theta_i = 0°; \phi_s = 0° \theta_s = 10°$).

As shown in Figure 9, the array is able to steer the beam to the desired direction even with phase quantization. As expected, the quantised version has a lower peak than the unquantized array. This quantisation loss is aligned with literature, which indicates loss of around 0.2dB for a 3-bit quantisation [14,15,16].

6.1.2   Case 2: $\phi_i = 0°, \theta_i = 0°; \phi_s = 0° \theta_s = 40°$

Another design aims to scatter the plane wave to $\theta_s = 40°$. The simulated bistatic RCS is shown in Figure 10. Besides producing the main lobe at $\boldsymbol{\theta_s} = 40°$ as desired, there is a significant high lobe at $\boldsymbol{\theta_s} = -58.5°$. It can be shown that this is a grating lobe.
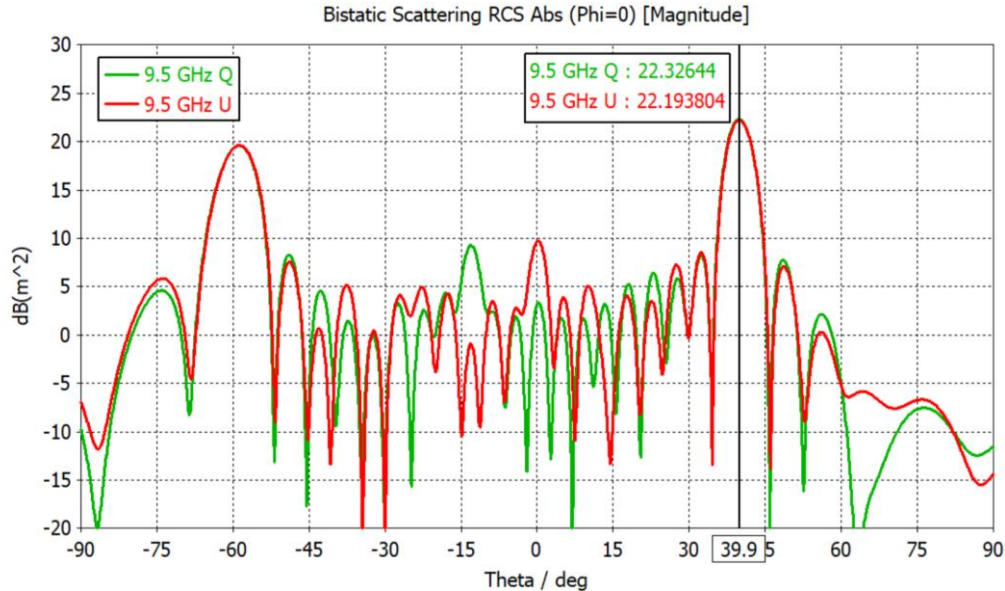

Figure 10: Simulated bistatic RCS of waveguide array ($\phi_i = 0°, \theta_i = 0°; \phi_s = 0° \theta_s = 40°$)

6.1.3   Case 3: $\phi_i = 0°, \theta_i = -30°; \phi_s = 0°, \theta_s = 45°$

For this case, the array is designed to deflect an incident plane wave from $\phi_i = 0°$, $\theta_i = -30°$ to the direction of $\phi_s = 0°$, $\theta_s = 45°$. The bistatic RCS is simulated and the results in Figure 11 show the desired deflected beam at 45°. Again, there is a grating lobe at -52.7°. The simulated *monostatic* RCS is shown in Figure 12.
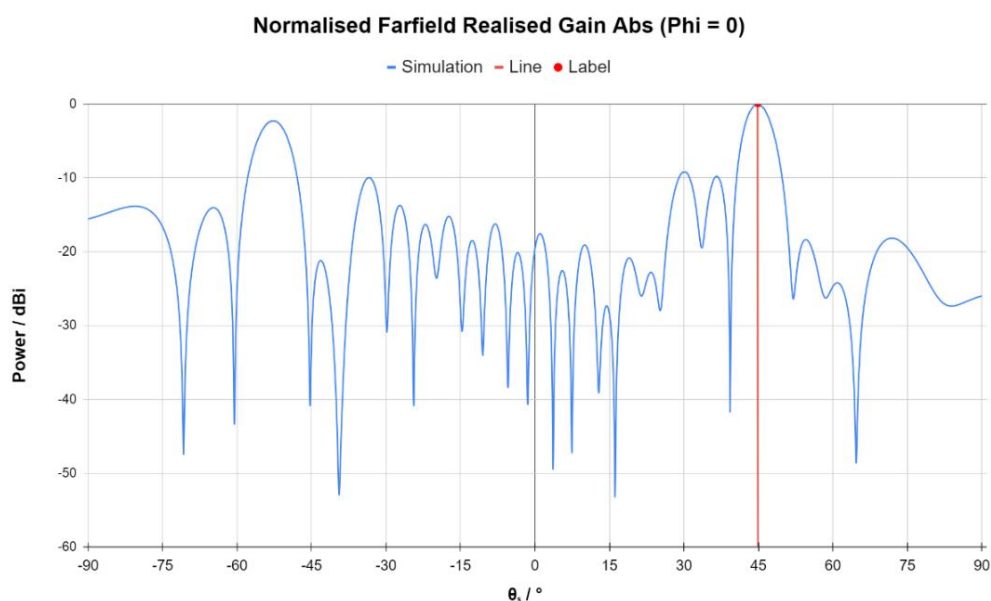

Figure 11: Simulated bistatic RCS of waveguide array ($\phi_i = 0°, \theta_i = -30°; \phi_s = 0°, \theta_s = 45°$)

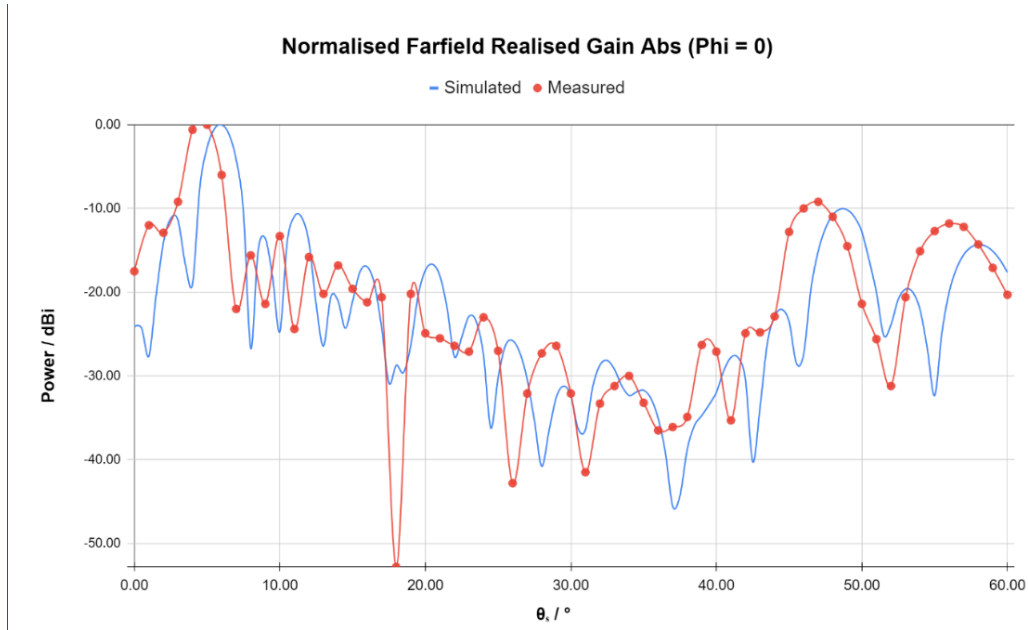Figure 12: Simulated monostatic RCS of waveguide array ($\phi_i = 0°$, $\theta_i = -30°$; $\phi_s = 0°$, $\theta_s = 45°$)

6.1.4 Experimental Verification for Case 3

Due to facility limitations, the monostatic RCS measurement for case 6.1.3 was performed in an anechoic chamber as shown in Figure 13. The measured (uncalibrated) results are superimposed over the simulated results in Figure 12. Owing to the manual alignment of the setup and the rotation arm, there is an angular offset in the measured results. Otherwise, the measured major peaks agree fairly well with the simulated peaks. It was not easy to capture the positions of the nulls accurately owing to the manual angular adjustment.
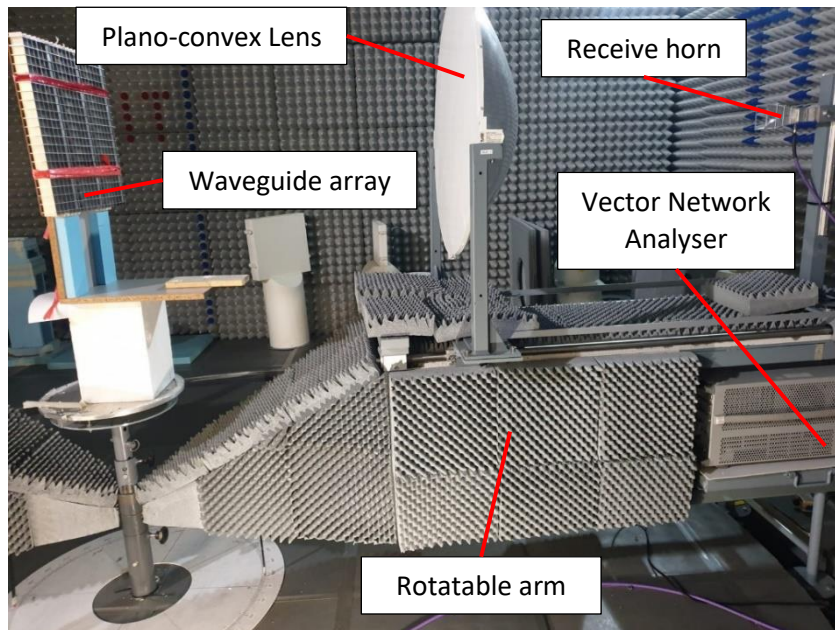

Figure 13: Experimental set-up for monostatic RCS measurement of waveguide array.

6.2   Radiation

The waveguide array can also be reconfigured as a reflectarray antenna. The simulated (normalized) radiation pattern of the reflectarray of 3.2.3 is shown in Figure 14. The quantized and unquantized results are fairly similar. The major differences are seen in the sidelobes.

To verify the results, the physical prototype with a feedhorn was measured in the same anechoic chamber for a limited angular span of -25° to 25°. The shape of the main beam for the simulated and measured results is in good agreement, as shown in Figure 15. The differences in the sidelobes shape can be attributed to the coarse tuning of the rotatable arm supporting the receiver. It was also noticed after all the measurements were done that the flat surface of the plano-convex lens was slightly tilted by 2° from the vertical. This tilt is another source of measurement error.
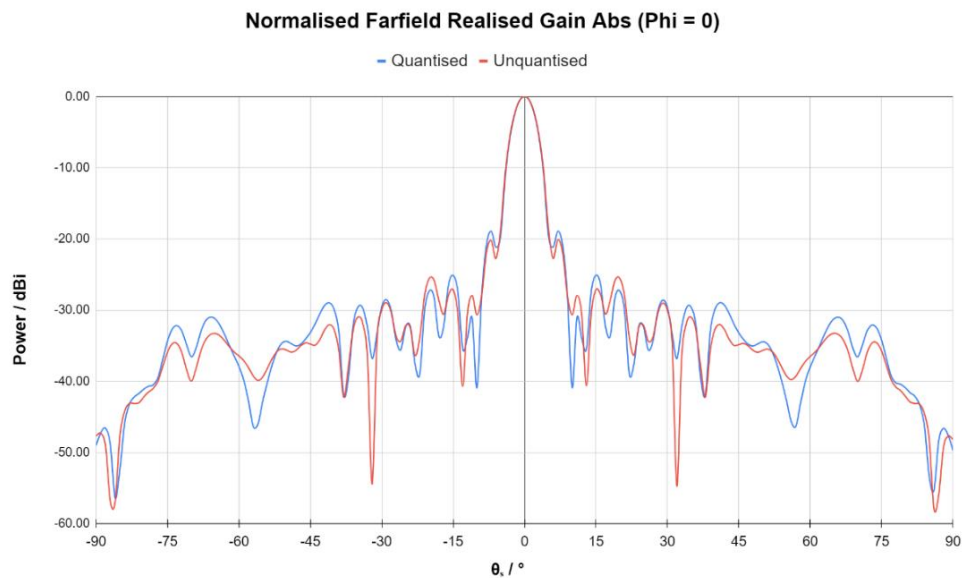

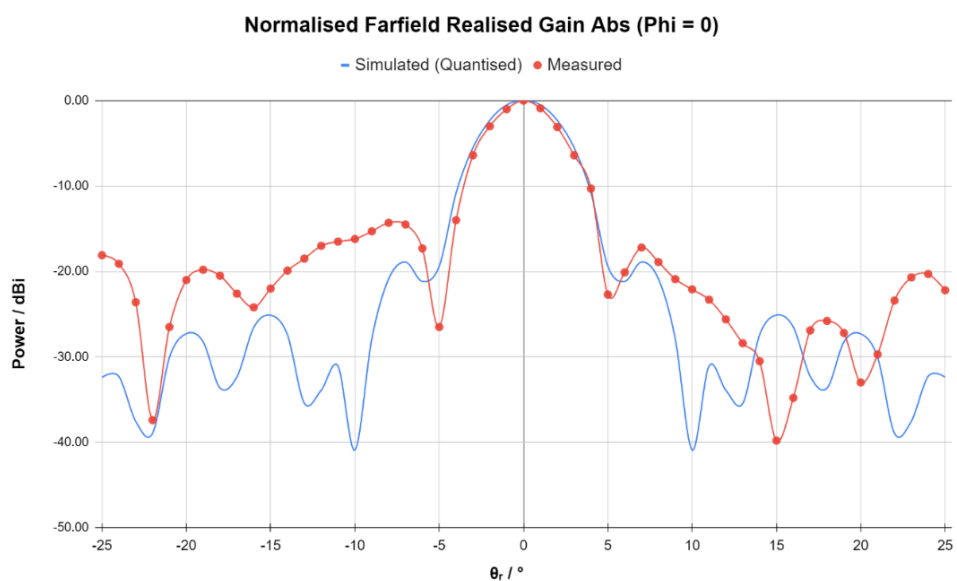Figure 14: Simulated radiation pattern of waveguide reflectarray.

Figure 15: Measured and simulated radiation pattern of waveguide reflectarray

7. Conclusion

We presented a 20x20 reconfigurable X-band waveguide array that can be used to study scattering and radiation. 3-D printing was used in the fabrication of the support for the phase-shift elements in the unit cells. Simulations and experimentations of various waveguide arrays were conducted to demonstrate the reconfigurable waveguide array. Specifically, we demonstrated scan angles of up to 45° for scattering control. We also demonstrated the use of the waveguide array as a reflectarray antenna. While providing beam scanning capabilities, the reconfigurable waveguide array is cost-effective and light. However, the manual reconfiguration of the array is tedious. An electro-mechanical system is proposed to replace the manual reconfiguration process.

References
[1]   Britannica, T. Editors of Encyclopaedia (2011, May 27). waveguide. Encyclopedia Britannica. https://www.britannica.com/technology/waveguide
[2]   G. -L. Huang, S. -G. Zhou, C. -Y. -D. Sim, T. -H. Chio and T. Yuan, "Lightweight Perforated Waveguide Structure Realized by 3-D Printing for RF Applications," in IEEE Transactions on Antennas and Propagation, vol. 65, no. 8, pp. 3897-3904, Aug. 2017, doi: 10.1109/TAP.2017.2715360.
[3]   J. Tak, A. Kantemur, Y. Sharma and H. Xin, "A 3-D-Printed W-Band Slotted Waveguide Array Antenna Optimized Using Machine Learning," in IEEE Antennas and Wireless Propagation Letters, vol. 17, no. 11, pp. 2008-2012, Nov. 2018, doi: 10.1109/LAWP.2018.2857807.
[4]   J. Huang and J. A. Encinar, Reflectarray Antennas, by Institute of Electrical and Electronics Engineers, John Wiley & Sons, 2008.
[5]   M. Zhang, J. Hirokawa and M. Ando, "A Four-Way Divider for Partially-Corporate Feed in an Alternating-Phase Fed Single-Layer Slotted Waveguide Array," in IEEE Transactions on Antennas and Propagation, vol. 56, no. 6, pp. 1790-1794, June 2008, doi: 10.1109/TAP.2008.923313.
[6]   S. M. A. Momeni Hasan Abadi, K. Ghaemi and N. Behdad, "Ultra-Wideband, True-Time-Delay Reflectarray Antennas Using Ground-Plane-Backed, Miniaturized-Element Frequency Selective Surfaces," in IEEE Transactions on Antennas and Propagation, vol. 63, no. 2, pp. 534-542, Feb. 2015, doi: 10.1109/TAP.2014.2381231.
[7]   Cadence System Analysis. (n.d.-a). Phased Array Antennas: Principles, Advantages, and Types. Cadence. Retrieved December 28, 2023, from https://resources.system-analysis.cadence.com/blog/msa2021phased-array-antennas-principles-advantages-and-types
[8]   S. Gao, Y. J. Guo, S. A. Safavi-Naeini, W. Hong and X. -X. Yang, "Guest Editorial Low-Cost Wide-Angle Beam-Scanning Antennas," in IEEE Transactions on Antennas and Propagation, vol. 70, no. 9, pp. 7378-7383, Sept. 2022, doi: 10.1109/TAP.2022.3208790.
[9]   Pini, A., [Art Pini]. (2019, August 28). The Fundamentals of RF Power Dividers and Combiners. DigiKey. Retrieved December 28, 2023, from https://www.digikey.com/en/articles/the-fundamentals-of-rf-power-dividers-and-

combiners#:~:text=Its%20major%20disadvantage%20is%20power%20loss%20via%20the,the%20resistive%20power%20divider%20use%20relatively%20low%20power

[10] Polo-López L, Masa-Campos JL, Ruiz-Cruz JA. Reconfigurable H-plane waveguide phase shifters prototyping with additive manufacturing at K-band. *Int J RF Microw Comput Aided Eng*. 2019; 29:e21980. https://doi-org.libproxy1.nus.edu.sg/10.1002/mmce.21980

[11] C. Liu, F. Yang, S. Xu and M. Li, "An E-Band Reconfigurable Reflectarray Antenna Using p-i-n Diodes for Millimeter-Wave Communications," in IEEE Transactions on Antennas and Propagation, vol. 71, no. 8, pp. 6924-6929, Aug. 2023, doi: 10.1109/TAP.2023.3291087.

[12] F. Venneri, S. Costanzo and G. Di Massa, "Design and Validation of a Reconfigurable Single Varactor-Tuned Reflectarray," in IEEE Transactions on Antennas and Propagation, vol. 61, no. 2, pp. 635-645, Feb. 2013, doi: 10.1109/TAP.2012.2226229.

[13] Nayeri, P., Yang, F., & Elsherbeni, A. Z. (2018). Reflectarray antennas [Wiley Online Library]. John Wiley & Sons Ltd. https://doi.org/10.1002/9781118846728

[14] H. Yang et al., "A Study of Phase Quantization Effects for Reconfigurable Reflectarray Antennas," in IEEE Antennas and Wireless Propagation Letters, vol. 16, pp. 302-305, 2017, doi: 10.1109/LAWP.2016.2574118.

[15] T. Debogovic and J. Perruisseau-Carrier, "Low Loss MEMS-Reconfigurable 1-Bit Reflectarray Cell With Dual-Linear Polarization," in IEEE Transactions on Antennas and Propagation, vol. 62, no. 10, pp. 5055-5060, Oct. 2014, doi: 10.1109/TAP.2014.2344100.

[16] Clénet, M., & Morin, G. (2000). Graphical investigation of quantisation effects of phase shifters on array patterns. ResearchGate, 23. https://www.researchgate.net/publication/235169396_Graphical_Investigation_of_Quantisation_Effects_of_Phase_Shifters_on_Array_Patterns